AIP | Applied Physics Letters

Tailoring light emission properties of organic emitter by coupling to resonance-tuned silver nanoantenna arrays

Teng Qiu, Fan Kong, Xiaoqiang Yu, Wenjun Zhang, Xianzhong Lang et al.

Citation: Appl. Phys. Lett. **95**, 213104 (2009); doi: 10.1063/1.3269190
View online: http://dx.doi.org/10.1063/1.3269190
View Table of Contents: http://apl.aip.org/resource/1/APPLAB/v95/i21
Published by the American Institute of Physics.

Tailoring light emission properties of organic emitter by coupling to resonance-tuned silver nanoantenna arrays

Teng Qiu,[1,a)] Fan Kong,[2] Xiaoqiang Yu,[1] Wenjun Zhang,[3] Xianzhong Lang,[1] and Paul K. Chu[3]
[1]*Department of Physics, Southeast University, Nanjing 211189, People's Republic of China*
[2]*School of Chemistry and Chemical Engineering, Southeast University, Nanjing 211189, People's Republic of China*
[3]*Department of Physics and Materials Science, City University of Hong Kong, Tat Chee Avenue, Kowloon, Hong Kong*

(Received 29 August 2009; accepted 8 November 2009; published online 25 November 2009)

A convenient nanotechnique is reported to tailor the light emission properties of organic emitter poly[2-methoxy-5-(2′-ethyl-hexyloxy)-*p*-phenylene vinylene] (MEH-PPV) by coupling to resonance-tuned silver nanoantenna arrays. It is revealed experimentally and theoretically that the enhanced photoluminescence from the MEH-PPV/silver nanoantenna complex may originate from the energy transfer effect in the surface plasmon resonance coupling between the MEH-PPV and silver nanocaps and from local electromagnetic field enhancement of nanogaps between the silver nanocaps in the background of the light-emitting MEH-PPV. The results are corroborated by the finite difference time domain simulation results. © *2009 American Institute of Physics*.
[doi:10.1063/1.3269190]

Since the early 1980s, enhancement of fluorescence from molecules near a metal nanostructure has been regarded to be associated with modification of the molecule excitation as well as the radiative and nonradiative decay rates.[1,2] Nowadays, improved nanofabrication methods allow precise control of the nanoparticle shape and arrangement of nanoparticle ensembles thereby opening the possibility to flexibly tailor specific molecule-nanoparticle couplings.[3,4] Popular approaches to obtain nanostructures which can provide increased light extraction (or collection) from emitters (or detectors) such as molecules, quantum dots, and wells or any photoactive materials include nanomanipulation with an atomic force microscopy probe, self assembly and lithography using focused ion beams, electron beams or nanoimprinting, microfabrication.[5–9] However, these processes can be laborious and costly and it is sometimes impossible to extend to large dimensions.

Herein, we report the fabrication of resonance-tuned silver nanocap arrays templated by porous anodic alumina (PAA) membranes as optical nanoantenna systems to support localized surface plasmon resonance (SPR) at optical frequencies. The use of PAA membranes as templates for the fabrication of the optical nanoantennae is especially promising considering the easy fabrication, excellent reproducibility, modest cost, and large area production, thereby boding well for applications in chip-level integration of optoelectronic devices such as photodetectors and light emitters. Considerable enhancement of photoluminescence (PL) from organic emitter poly[2-methoxy-5-(2′-ethyl-hexyloxy)-*p*-phenylene vinylene] (MEH-PPV) on silver nanoantenna arrays is observed. Moreover, the use of PAA membranes as the template to pattern the various periodic silver nanoantenna arrays offers more flexibility when spectrally tuning the SPR and controlling the ratio of scattering to absorption cross sections. Our results indicate that it is essential to optimize the geometry of the nanoantenna arrays in order to maximize the emission intensity.

High purity Al foils (99.99%) with a thickness of 0.2 mm were degreased by acetone and then electropolished in a mixture of ethanol and perchloric acid with a volume ratio of 5:1 under a constant dc voltage of 15 V for 3 min to further remove surface impurities. After rinsing in distilled water and drying, the Al foils were anodized separately in a 0.5 M oxalic acid solution under a constant dc voltage of 20, 30, 40, 50, or 60 V at 10 °C. In order to obtain an ordered nanopore array, we used a two-step anodizing process.[10,11] The Al foils were anodized for 2 h and then immersed into a mixture of chromic acid (1.8 wt %) and phosphoric acid (6 wt %) at 75 °C (1:1 in volume). After 2 h, the alumina layer was removed and the surface of the foil became bright. The anodizing time in the next step was 2 h. Afterwards, the PAA templates were obtained. Besides the ordered hexagonal pore array in the PAA templates, there were small protrusions along the surface of the pore wall and a dent existed between two neighboring protrusions. The three-dimensional (3D) geometry of the PAA substrate is shown schematically in Fig. 1(a), in which D, G1, G2, and G3 are the island (protrusion) diameter, ortho-, meta-, and paraisland (protrusion) gap, respectively. Such pores caused by volume expansion when aluminum is converted to alumina[10] can be used as the template to design and fabricate periodic silver nanoantenna arrays in which the areas exhibiting large gap-related fluorescence enhancement[12] are organized in a regular pattern. Afterwards, silver was deposited onto the surface of the PAA substrates in a direct-current magnetron-sputtering system. The magnetron power was ~40 W (voltage of 410 V and a current of 100 mA). The sputtering time of silver was 10 min. The typical nanoantennae structure shown in Fig. 1(b) is a 3D atomic force microscopy (AFM) (Vecco NanoScope V) image of the silver nanocap/PAA surface. This PAA membrane template was formed under a constant dc voltage of 40 V. The diameter of the pore was

a)Electronic mail: tqiu@seu.edu.cn.

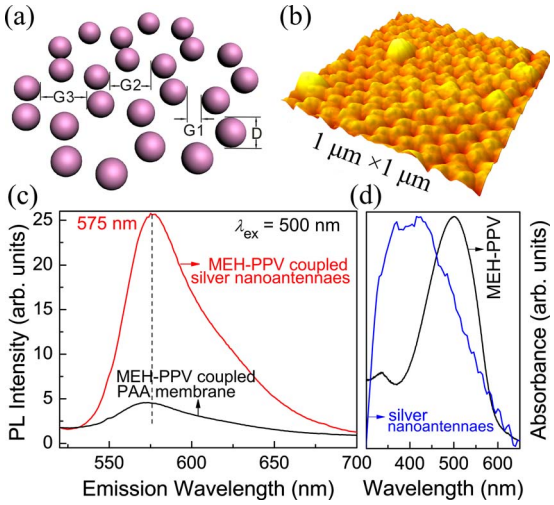

FIG. 1. (Color online) (a) Schematic representation of a 3D PAA surface with dimensional parameters D, G1, G2, and G3, where D is the island diameter and G1, G2, and G3 are the ortho-, meta-, and paraisland gap, respectively. (b) A typical 3D AFM image of the silver nanocap/PAA surface. (c) Comparison of PL spectra of the MEH-PPV coupled silver nanoantennae and MEH-PPV coupled PAA membrane. (d) Normalized UV-visible absorption spectra of the MEH-PPV and silver nanoantennae.

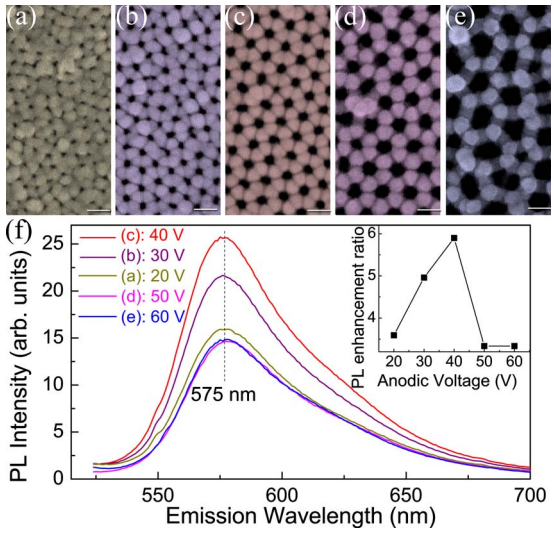

FIG. 2. (Color online) A series of SEM images acquired from the silver coated PAA membranes formed under different constant dc voltages: (a) 20 V, (b) 30 V, (c) 40 V, (d) 50 V, and (e) 60 V, respectively. Scale bar: 100 nm. The sputtering times of silver are all set to be 10 min. (f) PL spectra of MEH-PPV coupled silver nanoantennaes formed under different constant dc voltages [samples (a), (b), (c), (d), and (e) in Fig. 2]. The dependence of the PL enhancement ratio of MEH-PPV coupled silver nanoantennaes to MEH-PPV coupled PAA membrane is shown in the inset.

~35 nm. A protrusion with a diameter of ~50 nm occurred at each corner of one hexagonal cell. A concave shape could be observed between two neighboring protrusions.

MEH-PPV was chosen as the organic emitter because its optical property is well understood and has been widely applied to optoelectronic devices. The MEH-PPV powders were dissolved in a tetrahydrofuran solution to a concentration of 0.2 mg/ml at room temperature and then coupled to the silver nanoantennae by means of the drop coating of the solution onto the sample. The PAA membrane was cut into two pieces, one being a fresh sample and the other sputtered with Ag for 10 min to form the silver nanoantennae. The PL spectra of MEH-PPV coupled two samples are compared in Fig. 1(c) with the same acquisition time of 0.1 s acquired by excitation with the 500 nm line of a Xe lamp (Horiba Jobin Yvon Fluorolog-3). The peak intensity of the PL spectrum of the MEH-PPV coupled silver nanoantennae is about 6 times higher than that of the MEH-PPV on the PAA membrane and the PL peaks at 575 nm are almost the same. The enhancement of the PL efficiency of the MEH-PPV coupled silver nanoantennae may originate from the energy transfer effect in the SPR coupling.

The SPR-assisted PL enhancement is confirmed by the UV-visible absorbance spectra (LAMBDA 750) in Fig. 1(d). The π-π^* transition peaks at 500 nm from the MEH-PPV and large UV-visible absorption from 330 to 500 nm from the silver nanoantennae representing the surface plasmon energy, respectively, are observed. It should be noted that the large UV-visible absorption band of the silver nanoantennae is caused by the gaps with various sizes between neighboring silver nanocaps on the samples.[13] Similar to the donor acceptor energy matching in Förster resonance energy transfer between two fluorophores, the critical matching of the localized resonating plasmon energy (2.48–3.76 eV, equivalent to 330–500 nm) in silver nanoantennae with the electron transition energy from ground to excited state (2.16–3.1 eV, equivalent to 400–575 nm) in MEH-PPV permits the plasmon resonance energy transfer process. The quantized energy is likely transferred through the dipole-dipole interaction between the resonating plasmon dipole in nanoantennaes and the MEH-PPV dipole. Then, the resulting resonance (the SPR coupling due to the hybrid junction of MEH-PPV and the sliver nanoantennae) could lead to energy transfer from the sliver nanoantennae to the light-emitting MEH-PPV with the irradiating 500 nm line of Xe light, which created more excitons in the light-emitting MEH-PPV.[14]

Another important factor responsible for the increase in the luminescence efficiency may be local electromagnetic (EM) field enhancement of nanogaps between the silver nanocaps in the background of light-emitting MEH-PPV. To study this effect, the size of the gaps between neighboring silver nanocaps is altered by varying the anodic voltage of the PAA membrane templates. A series of scanning electron microscopy (SEM) (JEOL JSM-6335F) images taken from the silver coated PAA membranes formed at different anodic voltages are depicted in Figs. 2(a)–2(e). The sputtering time of silver is 10 min. These silver nanocaps cover the alumina protrusions and exhibit periodically hexagonal arrangements. Their sizes ($D=50\pm5$ nm) are quite similar due to the similar-shaped alumina protrusions and same sputtering time. The gaps (G1, G2) can be determined approximately by measuring G3 assuming that the array of six silver nanocaps is arranged in perfectly hexagonal disks. Thus, by varying the anodic voltage of the PAA templates, the nanopore expands or contracts while moving the deposited silver nanocaps closer or further together. The spacing can be tailored from less than 10 to 90 nm. Since the spacing between the nanocaps can be controlled by adjusting the anodic voltage, the local EM field enhancement can be tuned to achieve the strongest coupling between adjacent nanocaps. It should be noted that perfect self-organized growth which controls the nanopore arrangement occurs only under a certain anodic voltage. This is shown to be 40 V by our experiments [see Fig. 2(c)].

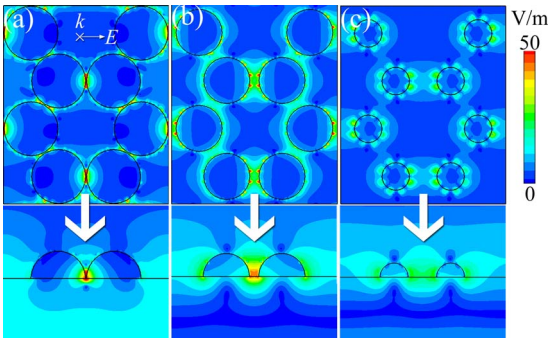

FIG. 3. (Color online) Simulated EM-field distribution maps of the silver nanoantennae arrays with different parameters. (a) D=50 nm G1=1 nm, (b) D=50 nm G1=10 nm, and (c) D=50 nm G1=50 nm. The inset in (a) shows the k-vector and polarization of the incident light in the simulation.

Figure 2(f) displays the PL spectra of MEH-PPV coupled silver nanoantennae formed at different constant dc voltages [samples (a)–(e) in Fig. 2], excited by the 500 nm line of a Xe lamp. The PL intensity increases slightly and then decreases sharply with increasing anodic voltages. The PL enhancement ratios are shown in the inset of Fig. 2(f) as a function of the anodic voltages. The maximum PL enhancement ratio (approximately six times) is observed from sample (c) in Fig. 2(c). Such a strong enhancement in sample (c) can be attributed to the fact that the nanoantenna array is assembled with the favorable gap configuration ($G3=\sim 35$ nm, $G2=\sim 25$ nm, $G1<10$ nm) as well as the highly ordered arrangement. This is necessary for intense PL enhancement as well as a high density of both Ag nanocaps ($\sim 1\times 10^{10}$ cm^{-2}) and hot gaps ($\sim 1\times 10^{11}$ cm^{-2}). Although mass particle aggregation in samples (a) and (b) [Figs. 2(a) and 2(b)] can be observed, the values of G2 and G3 decrease, thus not reducing the PL enhancement significantly. It can be further concluded that the larger interstitial sites in samples (d) and (e) [Figs. 2(d) and 2(e)] do not lead to enhanced PL.

In order to assess the relative contributions of different geometries to the experimentally observed PL intensities, the local EM-fields are calculated using commercial finite difference time domain (FDTD) software (RSOFT FULLWAVE). The array of silver nanoantenna is approximated by six hexagonally arranged hemispheres using dimensional parameters (D, G1, G2, G3) equal to the mean values of the samples produced experimentally. 500 nm light is assumed to be incident normal to the sample [inset in Fig. 3(a)]. Figure 3 mimics the situation of the samples fabricated at different constant dc voltages (the value of D is fixed at 50 nm whereas G1 increases from 1 nm to 50 nm). According to the contour plots of the near EM field distributions in Fig. 3, a larger enhancement is observed from a smaller gap size. The simulation results are in agreement with the studies reported by Wei *et al.*[15] as well as our experiments.

In summary, we have experimentally and theoretically demonstrated enhanced luminescence efficiency from MEH-PPV coupled to silver nanoantenna arrays. The enhanced PL from the MEH-PPV/silver nanoantennae complex originates from the energy transfer effect in the SPR coupling between the MEH-PPV and silver nanocaps and from local EM field enhancement of nanogaps between silver nanocaps in the background of a light-emitting MEH-PPV. The results are corroborated by FDTD simulation. This design incorporating silver nanoantennae arrays introduces a framework for the fabrication of robust, cost-effective, and large-area biochemical sensors, photodetectors as well as light emitters.

This work was supported jointly by the National Natural Science Foundation of China under Grant No. 50801013, the Specialized Research Fund for the Doctoral Program of Higher Education under Grant No. 200802861065, the Excellent Young Teachers Program of Southeast University and the Hong Kong Research Grants Council (RGC) General Research Fund (GRF) under Grant No. CityU 112307. The FDTD simulations are done at Nanjing University.

[1] J. Gersten and A. Nitzan, J. Chem. Phys. **75**, 1139 (1981).
[2] R. Ruppin, J. Chem. Phys. **76**, 1681 (1982).
[3] M. J. Banholzer, J. E. Millstone, L. D. Qin, and C. A. Mirkin, Chem. Soc. Rev. **37**, 885 (2008).
[4] H. Ko, S. Singamaneni, and V. V. Tsukruk, Small **4**, 1576 (2008).
[5] S. Gerber, F. Reil, U. Hohenester, T. Schlagenhaufen, J. R. Krenn, and A. Leitner, Phys. Rev. B **75**, 073404 (2007).
[6] J. Li, J. B. Xu, and H. C. Ong, Appl. Phys. Lett. **94**, 241114 (2009).
[7] J. H. Song, T. Atay, S. Shi, H. Urabe, and A. V. Nurmikko, Nano Lett. **5**, 1557 (2005).
[8] J. S. Biteen, N. S. Lewis, H. A. Atwater, H. Mertens, and A. Polman, Appl. Phys. Lett. **88**, 131109 (2006).
[9] K. Okamoto, I. Niki, A. Shvartser, Y. Narukawa, T. Mukai, and A. Scherer, Nature Mater. **3**, 601 (2004).
[10] J. P. O'Sullivan and G. C. Wood, Proc. R. Soc. London, Ser. A **317**, 511 (1970).
[11] S. Shingubara, O. Okino, Y. Sayama, H. Sakaue, and T. Takahagi, Jpn. J. Appl. Phys., Part 1 **36**, 7791 (1997).
[12] A. Bek, R. Jansen, M. Ringler, S. Mayilo, T. A. Klar, and J. Feldmann, Nano Lett. **8**, 485 (2008).
[13] E. Hutter and J. H. Fendler, Adv. Mater. (Weinheim, Ger.) **16**, 1685 (2004).
[14] M. S. Kim, D. H. Park, E. H. Cho, K. H. Kim, Q. H. Park, H. Song, D. C. Kim, J. Kim, and J. Joo, ACS Nano **3**, 1329 (2009).
[15] A. Wei, B. Kim, B. Sadtler, and S. L. Tripp, ChemPhysChem **2**, 743 (2001).